Effect of introduction of tetrabutylammonium bromide on properties of poly (L-lactic acid) tubular scaffold prepared by electrospinning

Chuan Jie Fan, Tian Shu Sun, Jing Qi Luo, Hai Yan Liu, Xiao Dong Zhou ✉

State Key Laboratory of Chemical Engineering, East China University of Science and Technology, Shanghai 200237, People's Republic of China
✉ *E-mail: xdzhou@ecust.edu.cn*

Published in Micro & Nano Letters; Received on 3rd September 2019; Revised on 16th November 2019; Accepted on 8th January 2020

In this work, poly (L-lactic acid) (PLLA) tubular scaffold was prepared by adding tetrabutylammonium bromide (TBAB) to the PLLA spinning solution. The effects of the introduction of TBAB on the morphology, crystallisation and mechanical properties of PLLA scaffolds were systematically studied by means of scanning electron microscope, differential scanning calorimetry (DSC), X-ray diffraction (XRD) and attenuated total reflectance Fourier-transform infrared spectroscopy. The results show that the introduction of TBAB improves crystallinity and mechanical property of the PLLA scaffold. As the TBAB content in the spinning solution increases, the mechanical properties of the PLLA tubular scaffold increase first and then decrease. The circumferential tensile strength of the PLLA tubular scaffold prepared by the spinning solution with addition of TBAB were found to increase by up to 323%. The results of DSC and XRD show that the introduction of TBAB can improve the crystallinity of the PLLA fibres. The Fourier-transform infrared spectroscopy test results demonstrate that the chain orientation of the PLLA fibres increases with the TBAB content in the spinning solution and induces the formation of α/α' crystal phase structure in the PLLA fibres, which is the main reason for the substantial improvement of the mechanical properties of the tubular scaffold.

1. Introduction: The main treatment for cardiovascular disease is vascular transplantation. However, due to the limited source of autologous blood vessels, research of artificial blood vessels has become a hot topic in recent years [1–3]. At present, large- and medium-caliber blood vessels have been studied and matured, whereas small-caliber blood vessels (diameter <6 mm) are prone to thrombosis during use. To solve the problem of embolisation of small blood vessels, much research effort has been devoted to the improvement of the preparation process and the selection of polymers [2, 4]. In this context, electrospinning technology has become a research hotspot for the development of biomaterials, since it can produce nano-sized porous structures that can effectively simulate the composition and structure of the extracellular matrix.

Polylactic acid (PLA) is a non-petroleum-based polymer with many excellent properties such as good biocompatibility, degradability and high mechanical strength and modulus, which explain its wide use in tissue engineering scaffolds, surgical sutures, drug carriers and other fields of biomedicine [5]. As a polycrystalline polymer, PLA properties such as mechanical, light transmission and gas barrier are related to its crystallinity and crystal structure. However, the PLA fibres prepared by electrospinning have low crystallinity [6], which results in low mechanical strength that limits its application. Consequently, many researchers have focused on the improvement of the mechanical properties of electrospun PLA fibres, developing approaches such as addition of nanoparticles [7], GO nanosheets [8] or PVA [9] to the spinning solution or adjusting the spinning parameters. Stretching in the processing of polymers has been revealed as an effective method to enhance their mechanical properties. This method can change the molecular chain motion and conformation of polymers, thereby altering their structure and properties. In their study on PLA tensile samples, Lv *et al.* [10] found that the molecular chains were oriented and conformed during the stretching process, and the mesophase appeared when the critical strain was reached. Meanwhile, Stocle *et al.* [11, 12] studied the crystallisation kinetics of PLA, focusing on the effects of strain and stretching temperature on the PLA structure. These studies indicate that the orientation and conformation of the molecular chains of PLA can be modified by increasing the tensile force on the PLA fibres during the electrospinning process, which would lead to PLA fibres having high crystallinity and concomitantly enhanced mechanical properties.

In this work, we aimed to increase the mechanical property of a PLLA tubular scaffold by adding tetrabutylammonium bromide (TBAB) to the spinning solution during the electrospinning process of PLLA fibres to improve the conductivity of the spinning solution. The effects of the introduction of TBAB on the fibre diameter, crystallisation properties and mechanical properties of the PLLA tubular scaffold are investigated.

2. Experimental

2.1 Materials: Semicrystalline poly (L-lactic acid) (PLLA, 2003D) was purchased from Natureworks. TBAB was purchased from Shanghai Macklin Biochemical Co., Ltd., China. Dichloromethane (CH_2Cl_2) and N, N-dimethylformamide (DMF), which were used as solvents, were purchased from Shanghai Lingfeng Chemical Regents Factory, China. The solvents were of analytical research grade and used without further purification.

2.2 Preparation and properties of spinning solutions: The PLLA solution (8% w/v) was prepared by dissolving PLLA in a solvent mixture of CH_2Cl_2/DMF at the volume ratio of 19/7 with and without the addition of TBAB (0, 0.1, 0.2, 0.4, 0.66, 0.8% w/v). The conductivity of these PLA solutions was measured by using a DDS-307W conductivity meter (Bante Instruments, Shanghai, China), and the viscosity was determined with a rotational viscometer (NDJ-8S, Shanghai Jitai Electronic Technology Co., Ltd., China).

2.3 Electrospinning process: The electrospinning setup is shown in Fig. 1. The PLLA solution was contained in a glass syringe with a plane tip of stainless steel needle having an inner diameter of 0.84 mm. The feeding rate of the PLLA solution into the tip was controlled at 1 ml/h using a syringe pump (LSP01-1A, Longer Precision Pump Co., Ltd, China). The applied voltage and the

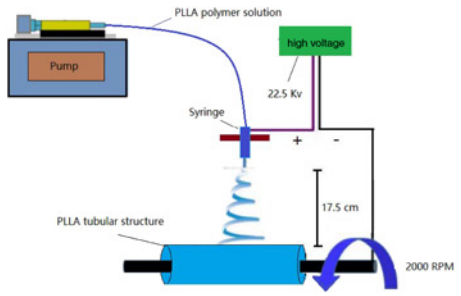

Fig. 1 *Schematic setup and optimised operation parameters for scaffold electrospinning*

distance between the tip and the collector were fixed at 22.5 kV and 17.5 cm, respectively. The electrospun PLLA fibres were collected on an aluminium foil that covered a rotating collector (2000 rpm). The electrospinning process was conducted at room temperature (15°C) and the relative humidity was controlled at 50%. After electrospinning, the samples were put into a vacuum oven at 15°C for two days to remove residual solvents. Finally, the samples were taken off and soaked in ethanol for two days to remove TBAB and then dried prior to testing.

2.4 Characterisation

2.5 Characterisation of the PLLA fibres: The morphology and diameter of the PLLA fibres were determined by using a scanning electron microscope (SEM, JSM-6360, FEI). The samples were mounted on adhesive tape and sputtered with a thin layer of gold prior to SEM observation. The average diameter of the PLLA fibres was determined from more than 250 measurements of the random fibres by using an image analysis software (Motic image plus 2.0.) to analyse the SEM images.

2.6 Statistical analysis: Data were collected from triplicate samples and expressed as the mean ± standard deviation. The diameter of the fibres prepared in the absence or presence of TBAB was analysed using the independent samples test. The significance level was set at $p < 0.05$.

The chemical structure of the as-spun PLLA fibres was characterised by attenuated total reflectance Fourier-transform infrared spectroscopy (ATR-FTIR) (Nicolet 6700, Thermo Electron Corporation) with a wavenumber range of 400–4000 cm^{-1}.

Differential scanning calorimetry (DSC) measurements were carried out using a temperature-modulated DSC Perkin Elmer instrument (Diamond DSC) under nitrogen atmosphere (50 ml/min). About 5 mg of samples were hermetically sealed in an aluminium pan for these measurements. The samples were heated from 40 to 200°C at a rate of 10°C/min, held for 3 min at 200°C, and then cooled down to 40°C at the same rate.

X-ray diffraction (XRD) measurements were carried out on a RIGAKU D/MAX 2550 instrument (Cu Ka radiation). The XRD data were collected between 5° and 40° in steps of 0.004° with an X-ray generator at 0.154 nm.

2.7 Mechanical characterisation: (i) *Circumferential tensile strength:* The circumferential tensile strength of the tubular scaffolds was tested according to the method provided in ISO 7198:2016. The tubular scaffold was cut into a 10 mm long sample and inserted between two copper tubes with an outer diameter of 2 mm. A copper wire was inserted into the copper tube and clamped. A schematic diagram of the test setup is shown in Fig. 2.

Prior to testing, all samples were placed in a 37°C electric thermostatic drying oven for 24 h to eliminate environmental effects. The flattening thickness of the tubular scaffold was

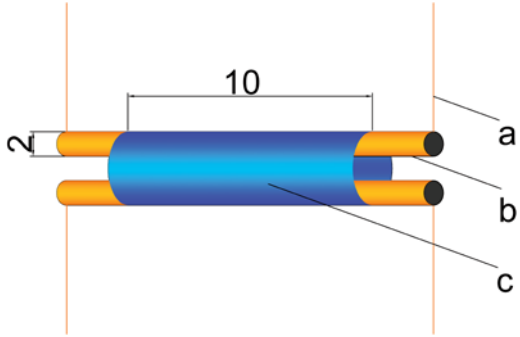

Fig. 2 *Schematic diagram of circumferential tensile strength, where a is a brass wire having a diameter of 0.8 mm, b is a brass tube having an outer diameter of 2 mm and an inner diameter of 1 mm, and c is a tubular scaffold with an inner diameter of 4 mm*

measured by a spiral micrometer. The tensile speed was set to 10 mm/min during the measurement, and at least five samples were tested in each set of experiments. The radial tensile strength was calculated according to the following formula:

$$\sigma_t = F_t/(b^*d) \tag{1}$$

where σ_t is the circumferential tensile strength, F_t is the maximum tensile load, b is the original length of the sample and d is the original thickness of the sample.

(ii) *Longitudinal tensile strength:* The longitudinal tensile strength of the tubular scaffold sample was tested according to the method provided in ISO 7198:2016. The tubular scaffold was cut into 40 mm long samples. All samples were placed in a 37°C electric thermostatic drying oven for 24 h before testing to eliminate environmental effects. The clamping length during the measurement was 20 mm, the stretching speed was 10 mm/min, and at least five samples were tested in each set of experiments.

The longitudinal tensile strength was calculated using the following formula:

$$\sigma_t = F_t/(b^*d) \tag{2}$$

where σ_t is the axial tensile strength, F_t is the maximum tensile load, b is the original width of the sample and d is the original thickness of the sample.

3. Results and discussion

3.1. Effect of the introduction of TBAB on the morphology and diameter of the PLLA fibres: Fig. 3 shows a SEM picture of the PLLA fibres prepared by adding different amounts of TBAB. From Fig. 4 it can be extracted that the diameter of the obtained PLLA fibres decreases first and then increases slightly as the TBAB content in the spinning solution increases. The diameter of the PLLA fibres reaches a minimum at a TBAB concentration of 0.66 w/v%. This may be due to the fact that the introduction of TBAB increases the conductivity and the viscosity of the spinning solution, as can be seen in Fig. 5. It is also shown that, under low TBAB concentration condition, the conductivity of the solution is greatly increased, whereas the viscosity is not significantly altered. Under these conditions, due to the increase of the conductivity of the solution, the electric field force of the formed solution jet dominates, which is advantageous for the reduction of the fibre diameter. As the content of TBAB increases further, the viscosity of the spinning solution increases up to a point in which the viscosity of the formed solution jet dominates, thereby suppressing the stretching of the jet by the electric field force and increasing the diameter of the resulting fibre. To explain the increase of the fibre diameter with TBAB concentration, the following reason

doi: 10.1049/mnl.2019.0544

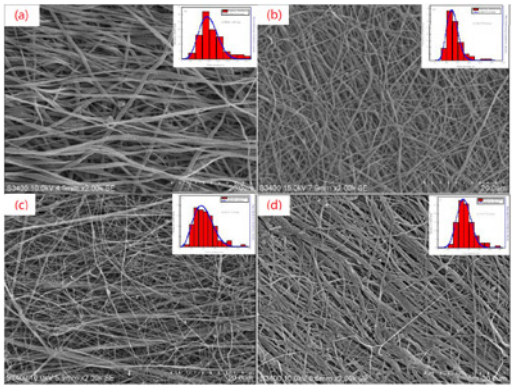

Fig. 3 *SEM pictures and fibre diameter distribution of the as-spun PLLA fibres with varying amounts of TBAB (w/v)*
a 0%
b 0.4%
c 0.66%
d 0.8%

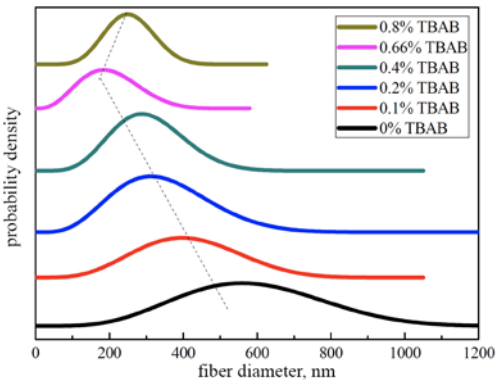

Fig. 4 *Histograms of normal distribution of the PLLA fibres prepared with varying concentrations of TBAB*

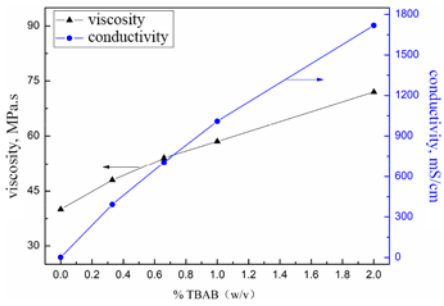

Fig. 5 *Influence of the amount of TBAB in PLLA/DCM/DMF solutions on viscosity and electrical conductivity*

can be also envisaged: At high TBAB concentrations, the electric field strength of the spinning solution is too high, resulting in a too high spinning speed that decreases the shortening time, with the concomitant increase in the fibre diameter. Furthermore, when the TBAB concentration exceeds 0.8 w/v%, the conductivity of the spinning solution is too high, and corona discharge such as electric spark and electro-acoustic sound occurs at the tip of the spinning needle, which may hinder the spinning process. Therefore, in this work, the concentration of TBAB was kept below 0.8 w/v%.

3.2. Effect of the introduction of TBAB on the mechanical properties of the PLLA tubular scaffold: Fig. 6 shows the tensile

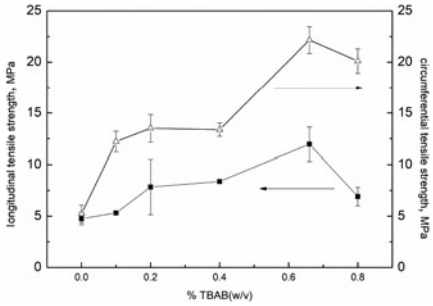

Fig. 6 *Strength of the as-spun PLLA tubular scaffold prepared with different TBAB concentrations*

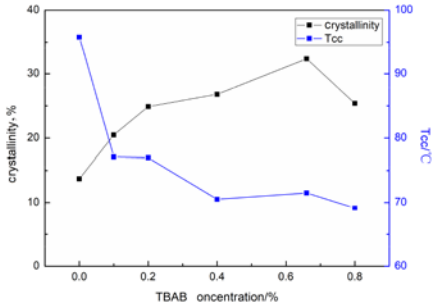

Fig. 7 *Plots of Xc derived from DSC thermograms against TBAB concentration*

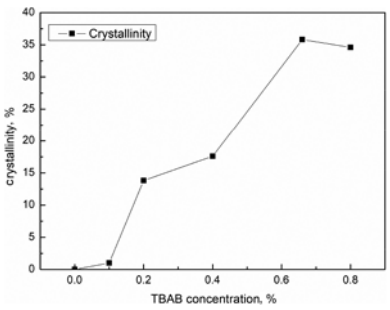

Fig. 8 *Plots of Xc derived from XRD against TBAB concentration*

strength test results of the PLLA tubular scaffold prepared with different TBAB contents. It can be seen from the figure that the circumferential and longitudinal tensile strength of the tubular scaffold gradually increase with the TBAB concentration, reaching a maximum at the TBAB content of 0.66 w/v%. Under this TBAB content, the longitudinal and circumferential tensile strength of the PLA tubular scaffold were found to increase by 152 and 323% respectively. Then, the tensile strength of the PLLA artificial blood vessel begins to decrease as the TBAB content increases further. It can be seen that the trend of tubular scaffold mechanical properties is consistent with the trend of PLLA crystallinity (with the exception of 0.4% TBAB content, Figs. 7 and 8).

We know that changes in crystallinity will cause changes in the mechanical strength of PLLA fibres. However, the mechanical properties of tubular scaffold are not only related to the mechanical strength of individual fibres (although it is the most important factor), but also affected by other factors, such as the diameter and distribution of fibres, the intertwining between fibres, the macroscopic orientation of fibres in tubular scaffold and so on (seen in Fig. 9). Therefore, at 0.4% TBAB content, the increase in crystallinity is not very high (7%, relative to that of 0.2% TBAB content, Fig. 7), resulting in the mechanical properties of

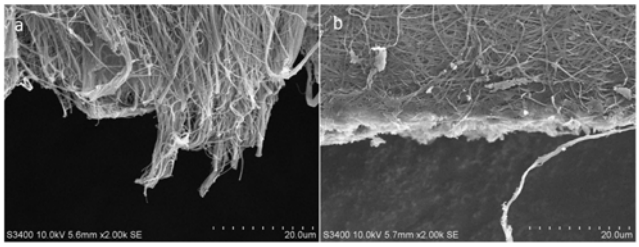

Fig. 9 *SEM pictures of PLLA tubular scaffold after*
a Circumferential tensile fracture
b Longitudinal tensile fracture

the tubular scaffolds not significantly increased or slightly decreased (Fig. 6). However, overall, the mechanical strength of the tubular scaffold increases as the crystallinity of the PLLA fibres increases.

3.3. DSC test: As a crystalline polymer, the macroscopic mechanical properties of PLLA correlate very well with its crystallinity and crystal structure. To investigate the effect of the introduction of TBAB on the crystallisation properties of the PLLA fibres, we performed a DSC analysis on the as-spun PLLA tubular scaffold.

Fig. 10 shows the DSC curves of the PLLA tubular scaffold. It can be seen that the glass transition temperature (T_g) of the sample without TBAB is about 60°C, and a broad cold crystallisation peak appears in the interval from 90 to 110°C due to the formation of imperfect crystals. Moreover, the cold crystallisation exothermic peak (Pcc) of the PLLA samples prepared with TBAB is smaller than that of the PLLA sample prepared in the absence of TBAB and is shifted to the low temperature direction. This phenomenon indicates that, in the PLLA sample prepared with TBAB, a crystal structure is formed during the stretching of the electrostatic field. It can also be seen from the graph that the endothermic peak appears after T_g (P_{endo}), which is mainly attributed to the melting of the mesogenic structure induced by tensile strain of the PLLA fibres in the electrostatic field during spinning [10]. Compared with the sample without TBAB, P_{endo} of the sample with TBAB was found to decrease, which may be due to the topological confinement effect of the crystal structure formed during spinning on the mesogen melting [12]. In addition, two melting peaks appear in the DSC curve of the PLA sample prepared without TBAB (T_m (1) = 143°C and T_m (2) = 154°C). Similar melting doublets have been observed in previous studies on the crystallisation of PLLA at 100 and 120°C [13]. The generation of the molten doublet in the DSC curve can be attributed to the melting/recrystallisation process at low heating rate, i.e. the imperfect crystal structure (α') has sufficient time to reconstitute the crystal with a higher orientation structure (α) and then remelts at

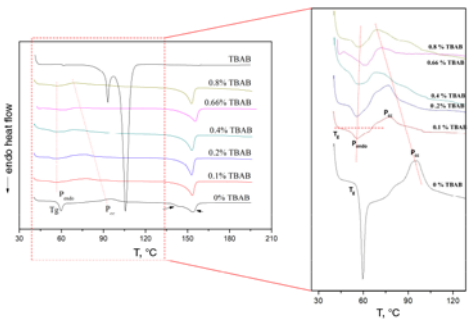

Fig. 10 *DSC curves (first heating scan) of the PLLA tubular scaffold prepared by using different TBAB concentrations (the right side of the figure is an enlarged view of the part in the dashed ellipse on the left side)*

higher temperature. However, upon addition of TBAB, the melting doublet did not appear on the DSC curve, which indicates that the addition of TBAB favours the conversion of α' crystal to α crystal.

Fig. 7 shows the curve of PLA crystallinity as a function of TBAB content. The crystallinity (Xc) of the PLA sample was calculated by the following formula:

$$Xc = \frac{\Delta Hm - \Delta Hcc}{\Delta H_{100}}$$

where ΔHm is the melting enthalpy of the sample, ΔH_{100} is the melting of 100% crystalline PLA, whose value is 93.1 J/g and ΔHcc is a cold crystallisation peak.

It can be seen from the figure that the PLA sample prepared without TBAB has lower crystallinity, which is consistent with the results of Xinhua Zhong *et al.* [6] on PLA fibres obtained by electrospinning process. In their work, this was attributed to the rapid evaporation of the solvent during electrospinning limiting the development of crystallisation. However, in our study, we found that the crystallinity of PLLA increased with the TBAB content in the spinning solution, reaching a maximum when the TBAB content was 0.66 w/v%, which is in accord with the results of the mechanical properties test. This suggests that the increase in crystallinity is the cause of the improvement of the mechanical properties of the PLLA tubular scaffold.

3.4. XRD test: To further investigate the crystalline structure of the PLLA tubular scaffold, we performed an XRD test. Fig. 11 shows the XRD spectra of the PLLA tubular scaffold. The XRD pattern of the PLA tubular scaffold prepared without adding TBAB is a broad and flat 'Taro' peak, indicating that the crystallinity of the sample is low. In contrast, as the TBAB content in the spinning solution increases, the broad scattering peak of amorphous phase becomes stronger and narrower and then develops into a sharp (200/110) peak of crystalline phase at about 16.5° 2θ. When the TBAB content was as high as 0.8%, a weak diffraction (203) peak appeared at 18.9° 2θ. By comparing the characteristic peaks of pure TBAB in Fig. 11, we can find that these two peaks are not from pure TBAB and should be caused by the change of PLLA crystal structure. This indicates that the crystalline phase formed in the PLLA tubular scaffold sample is that of a typical α crystal. Zhou *et al.* [14] found similar phenomena in the study of the effect of stretching rate on PLA crystallisation that with strain increasing the peak of (200/110) first appears and then the weak peak of 203 appears. Fig. 8 shows the crystallinity of the PLLA sample calculated from the XRD spectra as a function of the TBAB content. It can be seen that the crystallinity change of the PLLA sample is consistent with the DSC result.

3.5. ATR-FTIR test: Fig. 12 shows the changes in the infrared spectra of the PLLA tubular scaffold at different TBAB

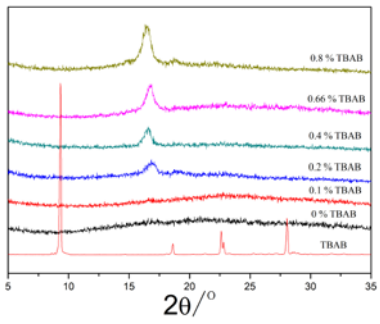

Fig. 11 *TBAB concentration dependence of XRD patterns*

doi: 10.1049/mnl.2019.0544

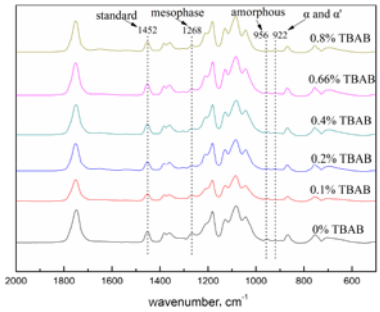

Fig. 12 *FTIR spectra of the tubular scaffold samples with different TBAB concentrations*

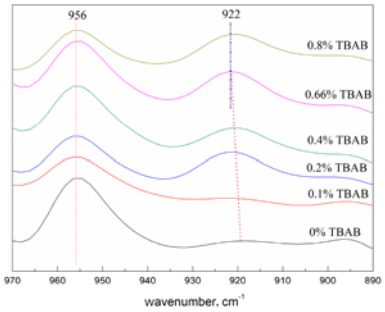

Fig. 14 *FTIR spectra of the tubular scaffold samples and peak position shifting versus TBAB concentration*

concentrations. The characteristic bands at 922, 956 and 1268 cm^{-1} correspond to the α/α' crystalline, amorphous and mesophase state in the PLA, respectively, which is in agreement with the reports by Stoclet *et al.* [11], Wasanasuk and Tashiro [15] and Na *et al.* [16]. The spectral analysis reveals that the characteristic band of α/α' crystals (922 cm^{-1}) is absent in the sample without TBAB, and a distinct crystalline band appears after the addition of TBAB. It can also be seen from the figure that the characteristic peak of the mesophase (1268 cm^{-1}) appears in the infrared spectra of PLLA regardless of the presence or absence of TBAB, which is also consistent with the results reported by Xinhua Zhong *et al.* [6]. They found that, although the PLA fibres obtained by spinning exhibit low crystallinity, a highly oriented intermediate phase structure (mesophase) occurs between the amorphous and crystalline states.

For the quantitative description of the influence of the introduction of TBAB on the crystalline state and mesophase content of the prepared PLA tubular scaffold, we selected the absorbance of the 1452 cm^{-1} characteristic peak in the infrared spectra as a reference by referring to the study by Piyawanee Jariyasakoolroj *et al.* [17]. The relative contents of I_{922}/I_{1452} and I_{1268}/I_{1452} in the infrared spectra of the PLA tubular scaffold prepared by spinning solution with different TBAB contents were calculated (Fig. 13), being I_{922} the intensity of the absorbance of the peak at α/α' crystal characteristic band (922 cm^{-1}), I_{1268} the intensity of the absorbance of the peak at mesophase characteristic band (1268 cm^{-1}) and the I_{1452} the intensity of the absorbance of the peak at 1452 cm^{-1}. It was found that the relative content of the α/α' crystalline region in PLA increases gradually with the TBAB content, reaching a maximum at a TBAB content of 0.66 w/w % that is followed by a slight decrease. This indicates that the introduction of TBAB is beneficial to the formation of α/α' crystals in PLA. Other researchers [17, 18] also found that it is precisely because of the increase of the α/α' crystal content in the PLA fibres that the mechanical properties of PLA are greatly improved. It can also be extracted from Fig. 13 that the relative content of the mesophase in PLA decreases gradually with the increase of the TBAB content in the spinning

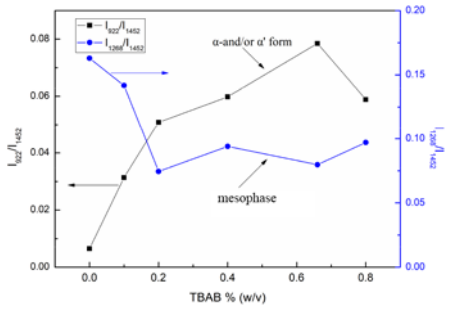

Fig. 13 *FTIR peak intensity ratios of crystalline phase and mesophase of various PLA fibres as a function of TBAB concentration*

solution, and then reaches a stable region. The observed trend of the α/α' crystalline region and the mesophase content in PLA suggests that the introduction of TBAB contributes to the transition from the highly oriented intermediate structure to the α/α' crystalline structure.

The change in absorbance of the characteristic band can reflect the change of crystallinity, but not the change of order of the PLA microstructure. Wasanasuk and Tashiro [15] and Hu [19] systematically studied the melt crystallisation and cold crystallisation behaviour of PLA. It was found that the characteristic band of the mesophase structure of PLA (918/919 cm^{-1}) shifted continuously to high wavenumber during the process of crystallisation. This shift represents the ordering process of the structure. The 918/919 cm^{-1} band is sensitive to conformational changes in the molecular chain; therefore, its shift can be correlated with the orderly adjustment of the conformation within the PLA molecular chain. In this Letter, the drift of the peak position corresponding to the ordered structure at 919 cm^{-1} can be used to reflect the molecular chain conformation adjustment upon introduction of TBAB into the PLLA electrospinning process. As can be seen in Fig. 14, as the TBAB content increases, the band at 919 cm^{-1} gradually shifts to a high wavenumber. This phenomenon indicates that the orientation of the intrachain conformation of the PLA molecule increases and eventually induces the formation of the α/α' crystal phase structure.

4. Conclusion: In this Letter, a high-performance PLLA tubular scaffold was prepared by adding TBAB to the PLLA spinning solution. The results show that the introduction of TBAB improves the conductivity and viscosity of the spinning solution. As the TBAB content in the spinning solution increases, the diameter of the prepared PLLA fibres decreases gradually before increasing slightly. This is mainly because the introduction of TBAB increases the electrical conductivity of the spinning solution and hence the electric field force of the jet formed by the spinning solution during electrospinning, which facilitates the reduction of the fibre diameter. The mechanical properties test reveals that the introduction of TBAB greatly increases the mechanical properties of the PLLA tubular scaffold. When the amount of TBAB is 0.66 w/v %, the circumferential tensile strength of the prepared PLLA tubular scaffold reaches a maximum (22.15 MPa). The mechanical properties of the PLA tubular scaffold prepared by the spinning solution with addition of TBAB were found to increase by up to 323%. The results of DSC and XRD show that the introduction of TBAB can improve the crystallinity of the PLLA fibres. The ATR-FTIR test results demonstrate that the chain orientation of the PLLA fibres increases with the TBAB content in the spinning solution and induces the formation of α/α' crystal phase structure in the PLLA fibres, which is the main reason for the substantial improvement of the mechanical properties of the tubular scaffold. Overall, the mechanical properties of PLLA tubular scaffold can be effectively improved by adding TBAB during the spinning

process, and the fabrication process was simple. We think these tubular scaffolds have notable clinical potential application in vascular tissue engineering. This work also has significant implications for fabrication of high-performance PLLA materials that use electrospinning method.

5 References

[1] Goins A., Webb A.R., Allen J.B.: 'Multi-layer approaches to scaffold-based small diameter vessel engineering: a review', *Mater. Sci. Eng. C, Mater.*, 2019, **97**, pp. 896–912

[2] Li X.D., Liu L.B., Zhang X.Z., *ET AL.*: 'Research and development of 3D printed vasculature constructs', *Biofabrication*, 2018, **10**, (3), p. 032002

[3] Hasan A., Memic A., Annabi N., *ET AL.*: 'Electrospun scaffolds for tissue engineering of vascular grafts', *Acta Biomater.*, 2014, **10**, (1), pp. 11–25

[4] Wu P.L., Nakamura N., Morita H., *ET AL.*: 'A hybrid small-diameter tube fabricated from decellularized aortic intima-media and electrospun fiber for artificial small-diameter blood vessel', *J. Biomed. Mater. Res. A*, 2019, **107**, (5), pp. 1064–1070

[5] Hadasha W., Bezuidenhout D.: 'Poly (lactic acid) as biomaterial for cardiovascular devices and tissue engineering applications' (Springer International Publishing AG, Cham, 2018), pp. 51–77

[6] Zong X., Kim K., Fang D., *ET AL.*: 'Structure and process relationship of electrospun bioabsorbable nanofiber membranes', *Polymer*, 2002, **43**, (16), pp. 4403–4412

[7] Dai J.M., Yang S.L., Jin J.H., *ET AL.*: 'Electrospinning of PLA/pearl powder nanofibrous scaffold for bone tissue engineering', *RSC Adv.*, 2016, **6**, (108), pp. 106798–106805

[8] Davoodi A.H., Mazinani S., Sharif F., *ET AL.*: 'GO nanosheets localization by morphological study on PLA-GO electrospun nanocomposite nanofibers', *J. Polym. Res.*, 2018, **25**, (9), p. 204

[9] Liu Y., Wei H., Wang Z., *ET AL.*: 'Simultaneous enhancement of strength and toughness of PLA induced by miscibility variation with PVA', *Polymers*, 2018, **10**, (10), p. 1178

[10] Lv R., Na B., Tian N., *ET AL.*: 'Mesophase formation and its thermal transition in the stretched glassy polylactide revealed by infrared spectroscopy', *Polymer*, 2011, **52**, (21), pp. 4979–4984

[11] Stoclet G., Seguela R., Lefebvre J.M., *ET AL.*: 'New insights on the strain-induced mesophase of poly (D, L-lactide): in situ WAXS and DSC study of the thermo-mechanical stability', *Macromolecules*, 2010, **43**, (17), pp. 7228–7237

[12] Stoclet G., Seguela R., Vanmansart C., *ET AL.*: 'WAXS study of the structural reorganization of semi-crystalline polylactide under tensile drawing', *Polymer*, 2012, **53**, (2), pp. 519–528

[13] Pan P., Kai W., Zhu B., *ET AL.*: 'Polymorphous crystallization and multiple melting behavior of poly(l-lactide): molecular weight dependence', *Macromolecules*, 2007, **40**, (19), pp. 6898–6905

[14] Zhou C.B., Li H.F., Zhang W.Y., *ET AL.*: 'Direct investigations on strain-induced cold crystallization behavior and structure evolutions in amorphous poly (lactic acid) with SAXS and WAXS measurements', *Polymer*, 2016, **90**, pp. 111–121

[15] Wasanasuk K., Tashiro K.: 'Structural regularization in the crystallization process from the glass or melt of poly (l-lactic acid) viewed from the temperature-dependent and time-resolved measurements of FTIR and wide-angle/small-angle X-ray scatterings', *Macromolecules*, 2011, **44**, (24), pp. 9650–9660

[16] Na B., Lv R., Zou S., *ET AL.*: 'Spectroscopic evidence of melting of ordered structures in the aged glassy poly(l-lactide)', *Macromolecules*, 2010, **43**, (4), pp. 1702–1705

[17] Jariyasakoolroj P., Tashiro K., Wang H., *ET AL.*: 'Isotropically small crystalline lamellae induced by high biaxial-stretching rate as a key microstructure for super-tough polylactide film', *Polymer*, 2015, **68**, pp. 234–245

[18] Tabi T., Hajba S., Kovacs J.G.: 'Effect of crystalline forms (alpha ' and alpha) of poly (lactic acid) on its mechanical, thermo-mechanical, heat deflection temperature and creep properties', *Eur. Polym. J.*, 2016, **82**, pp. 232–243

[19] Hu J., Zhang T., Gu M., *ET AL.*: 'Spectroscopic analysis on cold drawing-induced PLLA mesophase', *Polymer*, 2016, **53**, (22), pp. 4922–4926

doi: 10.1049/mnl.2019.0544